JOURNAL OF APPLIED ELECTROCHEMISTRY 23 (1993) 1251–1258

Ceramic electrodes for an alkali metal thermo-electric converter (AMTEC)

H. NAKATA, T. NAGATA, K. TSUCHIDA, A. KATO

Department of Chemical Science and technology, Faculty of Engineering, Kyushu University, Fukuoka 812, Japan

Received 19 October 1992; revised 1 April 1993

TiN, TiC, TiC/TiN, and Mo electrodes for an Alkali Metal Thermo-Electric Converter (AMTEC) were prepared by ceramic processing and their cathodic polarization characteristics were studied at 600–800° C. The polarization characteristics for TiN and TiC electrodes were similar to those for the Mo electrode. Among three kinds of TiC electrodes with different morphologies, the electrode consisting of finer grains gave a higher power density (0.40 W cm^{-2}). The activation energies for the exchange current density were smaller for ceramic electrodes than for the Mo electrode. In the high current density region above about 1 A cm^{-2}, a limiting current region appeared. When the vacuum level of the low temperature region, which was controlled by introduction of argon, was below 10 Pa, the power density did not depend on the vacuum level but, above 10 Pa, the power density decreased with increase of argon pressure.

1. Introduction

The Alkali Metal Thermo-Electric Converter (AMTEC) using β''-alumina solid electrolyte (BASE) is receiving increasing attention as a thermoelectric converter system of high efficiency and high power density [1–5]. The principle of AMTEC is shown in Fig. 1. AMTEC uses liquid sodium as an operating fluid and BASE as a separator. The driving force is the sodium activity difference between the high temperature region (600–1000° C) and the low temperature region (100–500° C). Liquid sodium (anode) becomes sodium ion to release an electron to the anode in the high temperature region, and sodium ions pass through the BASE toward the low temperature region. The sodium ion passing through the BASE receives an electron through an external circuit from the liquid sodium to form sodium vapour on the BASE/electrode interface. Sodium vapour flows from the electrode to the cooled surface where it condenses and is pumped back to the high temperature region. AMTEC has many advantages for terrestrial and space power application; power density and efficiency independent of size and no moving parts, little waste gas, etc. [1–5].

For AMTEC, a key issue is the development of a highly efficient electrode. So far, sputtered Mo electrodes have been studied widely as AMTEC electrodes. However, the oxide layer on the molybdenum reacts with sodium to form Na_2MoO_4. This compound vaporizes rapidly at temperature above 800° C, resulting in the degradation of its performance [6]. In order to find better electrode materials, the present authors investigated the reactivity of nitrides and carbides of transition metal (IV, V and VI groups) for BASE and liquid sodium [7]. As a result, TiN, TiC, NbN, and NbC were concluded to be good candidates as AMTEC electrode materials. Further, it was found that it is possible to prepare an electrode on BASE by a screen printing method from fine powders of TiN, TiC and NbN [8]. In the present work, the influence of the material and structure of the electrode on AMTEC performance was investigated.

2. Experimental details

2.1. *Preparation of electrodes*

TiN, TiC, TiC/TiN, and Mo [9] powders were mixed with the organic vehicle (terpineol + ethylcellulose (10 wt %)) and the resulting paste was painted onto β''-alumina tube (Ceramatec Inc., outer diameter: 15 mm, thickness: 1 mm, length: 200 mm) through a screen mesh (RISO Kagaku Co., Hi-mesh master, 200 mesh). The powder content in the paste was 20 wt %. The printed paste was dried at 150° C for 20 min in air and fired at 900 or 1000° C for 1 or 3 h in an Ar–H_2 (100: 500 ml min^{-1}) atmosphere or NH_3–H_2 (80: 20 ml min^{-1}) atmosphere. The powders used, and the firing conditions, are shown in Table 1. The thickness of these electrodes was in the range 3–5 μm.

2.2 *AMTEC apparatus*

The AMTEC apparatus used is shown in Fig. 2. The vessel was made of stainless steel. The upper chamber contained an argon atmosphere (1 atm) and the lower chamber was evacuated to 10^{-2}–10^{-1} Pa by means of an oil-diffusion pump. The upper and lower chambers were sealed by means of O-rings. About 6 g of sodium

0021-891X

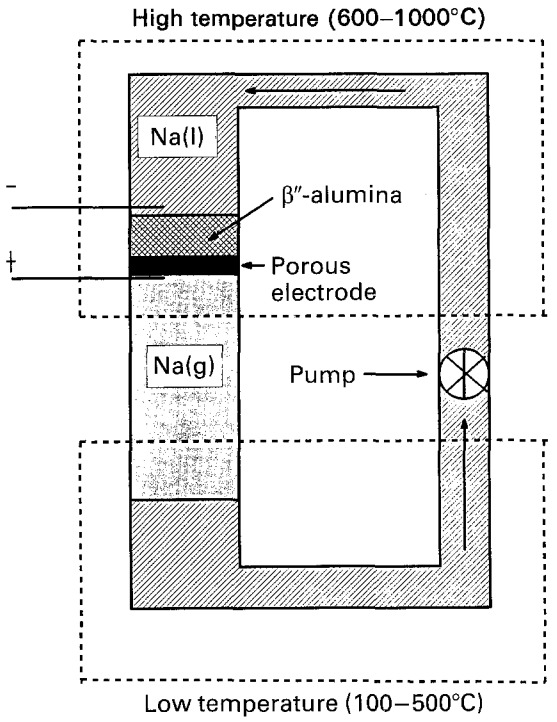

Fig. 1. Principle of AMTEC.

metal was introduced into the β''-alumina tube and was heated by both an inner heater and an outer heater. A small amount of Ti sponge was placed in the β''-alumina tube to prevent the oxidation of sodium. The temperatures of sodium metal in the β''-alumina tube, electrode, and the inner surface of the steel vessel were monitored by Chromel–Alumel thermocouples. The structure of the cell is shown in Fig. 3. Molybdenum mesh (30 mesh) was placed on the electrode and tied by molybdenum wires (diam. 0.3 mm) together with molybdenum wire (diam. 1 mm) as the current lead, molybdenum wire (diam 0.3 mm) as the voltage measuring lead, and a Chromel–Alumel thermocouple insulated by a α-alumina tube.

Table 1. Powders used as electrodes and firing conditions

Electrode	*Raw Powder*		*Firing condition*		
	Preparation	*Particle size/μm*	*Temp /°C*	*Atmosphere*	*Time /h*
TiN	Syn.[1]	<0.1	1000	NH_3–H_2	1
TiC–1	Syn.[2]	<1	1000	Ar–H_2	3
TiC–2	Syn.[2]	<1	900	Ar–H_2	3
TiC–3	Com.[3]	<10	1000	Ar–H_2	3
TiC/TiN	Com.[4]	<3	1000	H_2	3
Mo	Syn.[5]	<0.05	1000	H_2	1

[1] Synthesized TiN powder obtained by nitriding Ti powder (Vacuum Metallurgical Co., Ltd.) at 1000° C for 2 h in NH_3–H_2 atmosphere.
[2] Synthesized TiC powder obtained by carbonizing the Ti powder at 1000° C for 3 h in CH_4–H_2 atmosphere.
[3] Commercial TiC powder (Rare Metallic Co., Ltd).
[4] Commercial TiC/TiN powder (Japan New Metals Co., Ltd) consisted of mixture of both compounds.
[5] Synthesized molybdenum powder obtained by vapour phase reaction [9].

2.3. *Electrochemical measurement*

Voltage–current profiles were measured by cyclic-voltammetry (sweep rate: 5 mV s^{-1}) using a potentiostat (Hokuto Denko Co., Ltd HA-501G) and a function generator (Hokuto Denko Co., Ltd HB-105). Cell current and voltage were measured between the external wall of the inner heater and the current lead wire, and between the external wall of the inner heater and the voltage lead wire, respectively. Complex impedance analysis was made using a frequency response analyzer (Solartron FRA–1250A) and a potentiostat over the frequency range 65 kHz to 0.1 or 0.01 Hz. The current interrupt measurements were carried out using a function generator, a galvanostat (Hokuto Denko Co., Ltd HA-501G), and a digital storage scope (Hewlett Packard HP 54600A). All the measurements were controlled by a computer system (Epson PC-286VG + GPIB interface).

3. Results and discussion

3.1. *Effect of the electrode materials on the cathodic overvoltage*

Figure 4 shows the SEM images of various electrodes. The voltage–current profiles for these electrodes at 750° C are shown in Fig. 5. The maximum power densities were 0.18 W cm^{-2} for the TiN electrode, 0.24 W cm^{-2} for the TiC-2 electrode, 0.08 W cm^{-2} for the TiC/TiN electrode, 0.38 W cm^{-2} for the molybdenum electrode. The ohmic resistances of these cells were measured by both complex impedance and current interruption methods. The ohmic resistances obtained by both methods agreed well. Because the ohmic resistance differed considerably among the four electrodes, it was not possible to evaluate the characteristics of the electrode material from the power density alone. Thus, the cathodic overvoltage was calculated by using the ohmic resistance. The relation between current density and cathodic overvoltage at 750° C is shown in Fig. 6. Figure 6 shows that the polarization characteristics for TiN and TiC electrodes were nearly the same as those for the Mo electrode. However, the current density for the TiC/TiN electrode was much lower than that for the other electrodes, which may be due to large grains in this electrode. Similar current density–cathodic overvoltage relations were observed at 600, 650, 700 and 800° C. The relations were represented by Equation 1 taking into account both kinetic and mass transport effects at the β''-alumina/electrode interface [10],

$$I = I_0\left[\exp\left(-\frac{\alpha\eta F}{RT}\right) - \frac{\Delta P_e + \Delta P_{pe} + P_l}{P_l}\exp\left(\frac{(1-\alpha)\eta F}{RT}\right)\right] \quad (1)$$

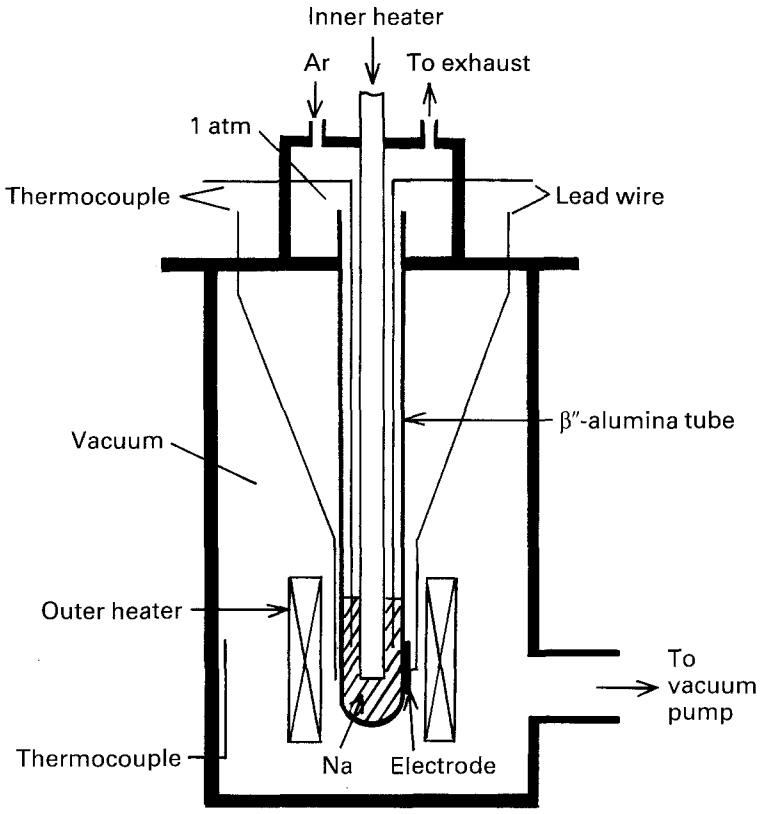

Fig. 2. Apparatus of AMTEC.

where:

$$\Delta P_e = (2\pi MRT)^{1/2} I/F$$
$$\Delta P_{pe} = 0.75 G (MRT/2\pi)^{1/2} I/F.$$

I, I_0, η, and α are the current density, exchange current density, overvoltage, and transfer coefficient, respectively. ΔP_e, ΔP_{pe} and P_l are pressure drop due to sodium flux from electrode surface, pressure drop in the electrode, and pressure drop due to evaporation of sodium from the condenser, respectively. F is the Faraday constant, M is molar weight of sodium, and G is a dimensionless geometrical parameter. When the cathodic overvoltage (η) is very low, Equation 1 is approximated by Equation 2.

$$I = I_0 \left[\left(1 - \frac{\Delta P_e + \Delta P_{pe} + P_l}{P_l} \right) \left(1 - \frac{\alpha \eta F}{RT} \right) - \left(\frac{\Delta P_e + \Delta P_{pe} + P_l}{P_l} \cdot \frac{\eta F}{RT} \right) \right] \quad (2)$$

When I is 5 mA cm^{-2} (at T_h (high temperature side) = 1023 K, T_l (low temperature side) = 473 K), the ratio, $(\Delta P_e + \Delta P_{pe} + P_l)/P_l$, becomes approximately 1. Thus, the exchange current densities (I_0) for each electrode were calculated by applying $I_0 = IRT/\eta F$ for the low overvoltage region.

Figure 7 shows an Arrhenius plot of the exchange current density. The activation energies of the electrode reaction were calculated as 47 kJ mol^{-1} for

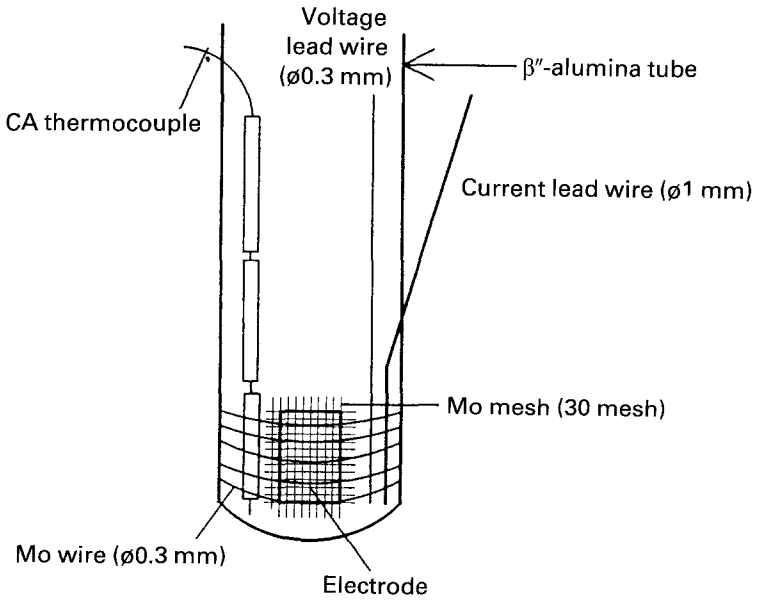

Fig. 3. Structure of cell.

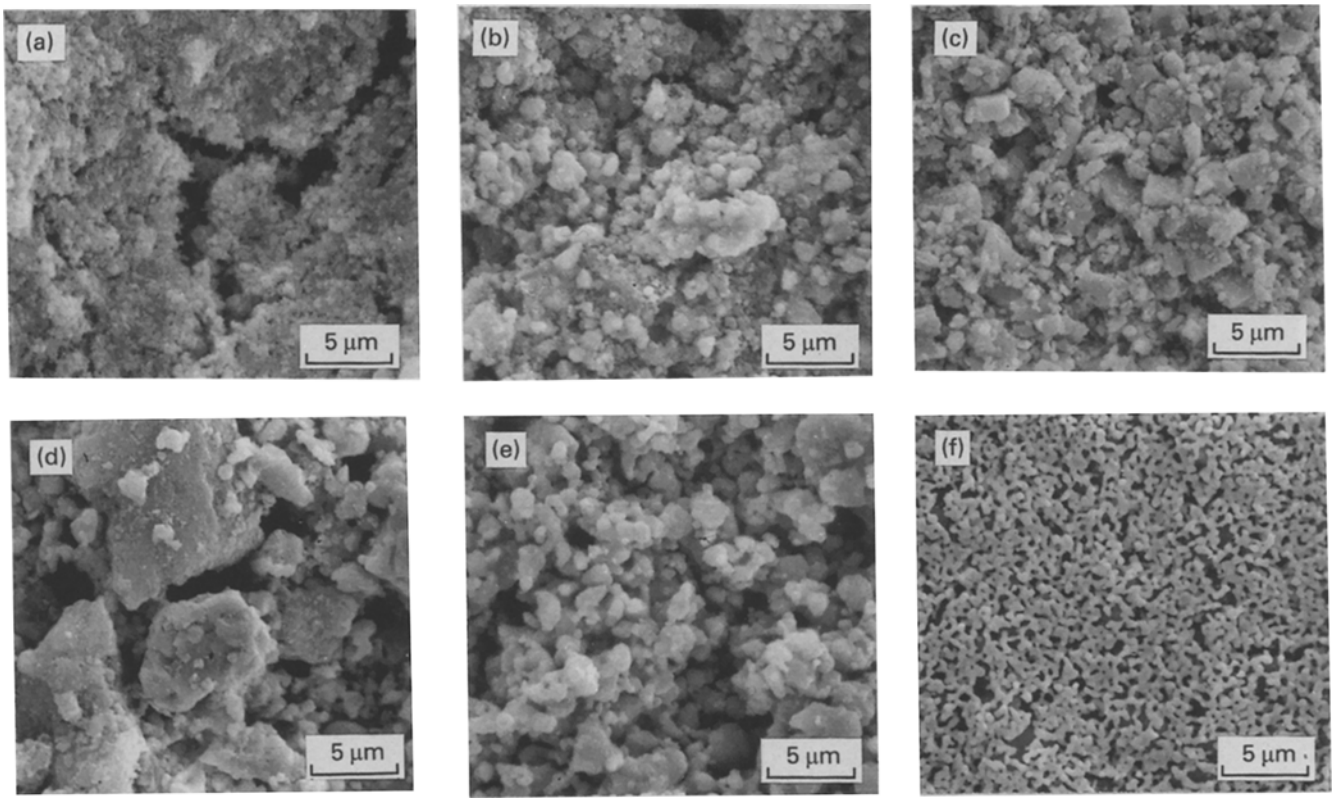

Fig. 4. SEM images of various electrodes (a) TiN, (b) TiC–1, (c) TiC–2 (d) TiC–3, (e) TiC/TiN and (f) Mo.

TiN, 43 kJ mol^{-1} for TiC–1, 67 kJ mol^{-1} for TiC–2, 56 kJ mol^{-1} for TiC–3, 68 kJ mol^{-1} for TiC/TiN, and 107 kJ mol^{-1} for molybdenum. It should be noted that the activation energies are lower for the ceramic electrode than for the molybdenum electrodes.

3.2. *Effect of the structure of the electrode on the cathodic overvoltage*

As seen from SEM images of three kinds of TiC electrodes in Fig. 4, the structure is considerably different among the three electrodes and the grain size increases in the order TiC–2 < TiC–1 < TiC–3. The grain size in the TiC–2 electrode is finer than that in the TiC–1 electrode because of a lower firing temperature. Figure 8 shows the cathodic overvoltage for three kinds of TiC electrodes at 750° C. The overvoltage for a given current density increases in the order TiC–2 < TiC–1 < TiC–3 which shows that electrode with finer grain size gives lower overvoltage. The

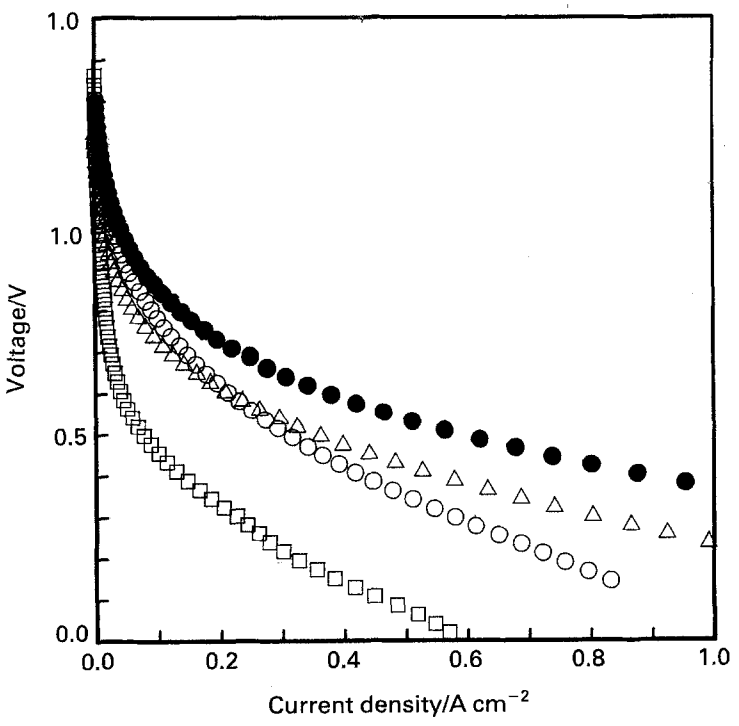

Fig. 5. Voltage–current profiles for various electrodes at 750° C. (Vacuum level: 0.5–0.02 Pa). Key: (○) TiN, (△) TiC–2, (□) TiC/TiN, (●) Mo.

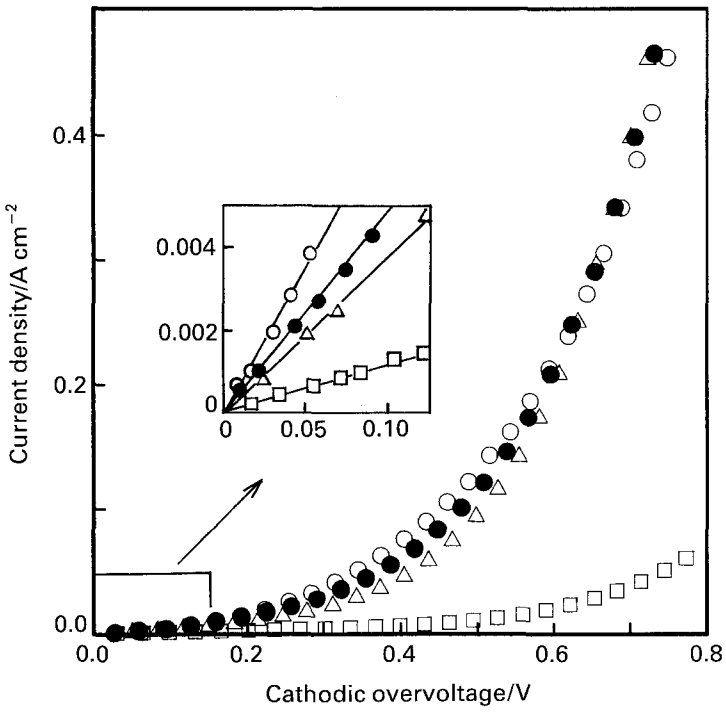

Fig. 6. Relation between overvoltage and current density of AMTEC at 750° C. Key: (○) TiN, (△) TiC–2, (□) TiC/TiN and (●) Mo

charge transfer process in the AMTEC cathode occurs at the triple-phase boundary of BASE/porous electrode/sodium gas. Consequently, the overvoltage decreases with increase in the length of the triple-phase boundary. The electrode with a finer grain size will have a longer triple-phase boundary. Among the three TiC electrodes, the length of the triple-phase boundary may be longest for the TiC–2 electrode and shortest for the TiC–3 electrode. Thus, an electrode with fine grain size is necessary to obtain a high current density.

Further, as can be seen in Fig. 9, the Tafel relation holds between the overvoltage and the logarithm of the current density below about 0.8 V (Electrode: TiC–2). However, a limiting current appears in the high current density region, indicating that mass transfer through the electrode becomes rate-determining. Figure 10 shows the impedance plots (Electrode: TiC–2) measured by the complex impedance method at the points (a) and (b) in Fig. 9. The impedance arc is a depressed semicircle due to both kinetic and mass transfer processes at the point (a). On the other hand, at the point (b), the impedance spectra is separated into two semicircles because of the difference of relaxation constant of the kinetic process and the mass transfer process.

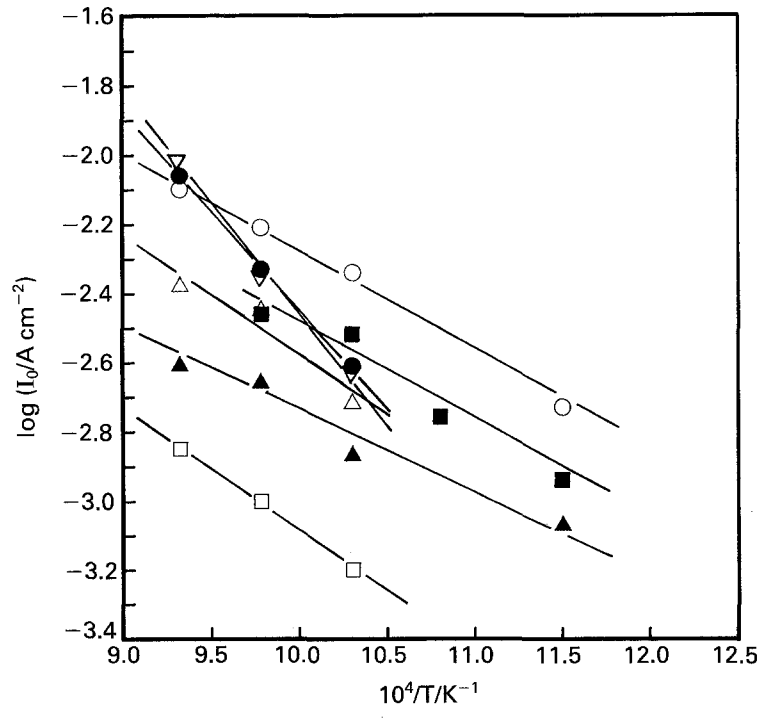

Fig. 7. Arrhenius plots of exchange current density (Mo(1): this work, Mo(2): JPL[11]). Key: (○)TiN, (▲) TiC–1, (△) TiC–2, (■) TiC–3, (□) TiC/TiN, (●) Mo(1) and (▽) Mo(2).

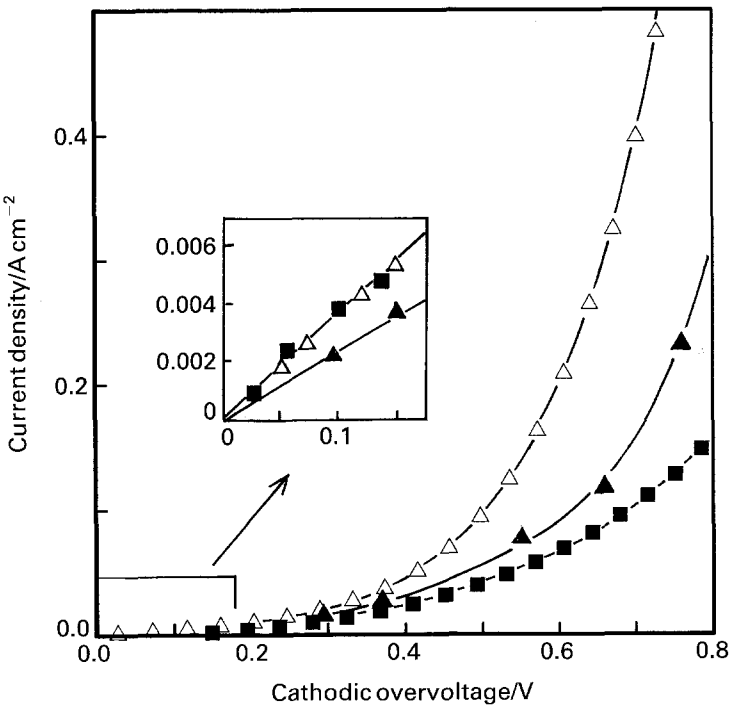

Fig. 8. Relation between overvoltage and current density of AMTEC with TiC electrode at 750° C. Key: (▲) TiC–1, (△) TiC–2 and (■) TiC–3.

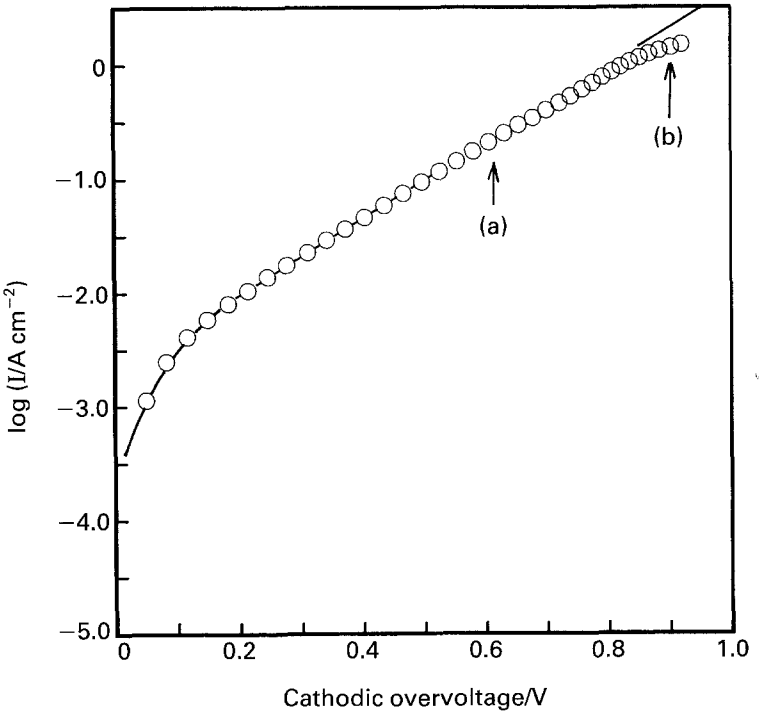

Fig. 9. Relation between overvoltage and logarithm of current density of AMTEC with TiC–2 electrode at 750° C. (—) Bulmer–Volmer equation (I_0 = 3.5 mA cm^{-2}, α = 0.59).

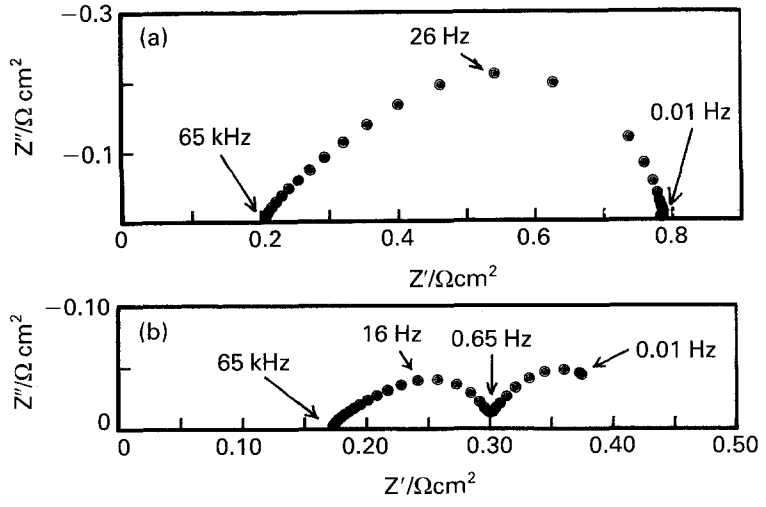

Fig. 10. Complex impedance plots of AMTEC with TiC–2 electrode at 750° C ((a) and (b): see Fig. 9).

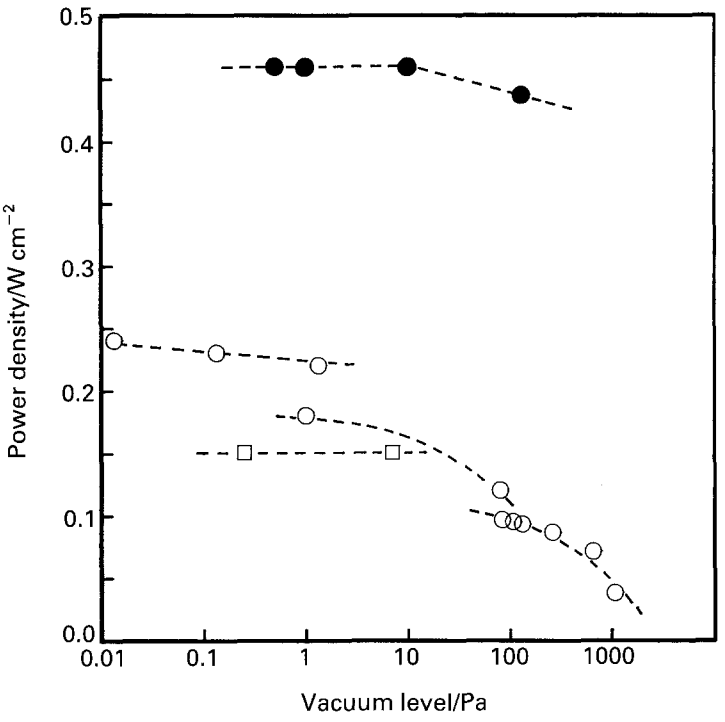

Fig. 11. Effect of vacuum level on the power density at 800° C. (Vacuum level was controlled by introduction of argon). Key: (○) TiN, (□) TiC/TiN and (●) Mo.

Consequently, a moderate porosity is necessary for an AMTEC electrode to obtain a high current density.

3.3 *Effect of the vacuum level on the power density*

Figure 11 shows the effect of vacuum level on the power density for TiN, TiC/TiN, and Mo electrodes at 800° C. At 800° C, the vacuum level gives little effect on the power density below 10 Pa, but above 10 Pa the power density decreases as the vacuum level becomes poor. Assuming a representative length of the flow (L_M) as 10 μm, the Knudsen number (λ/L_M, λ: mean free path) becomes 200–300 at 10 Pa. Consequently, the flow of sodium vapour is free molecular flow below 10 Pa, but is affected by viscous flow above 10 Pa.

3.4. *Mechanism of the electrode reaction*

For the electrode reaction in the present cell, the following four steps are considered. The schematic model for the electrode reaction is given in Fig. 12.

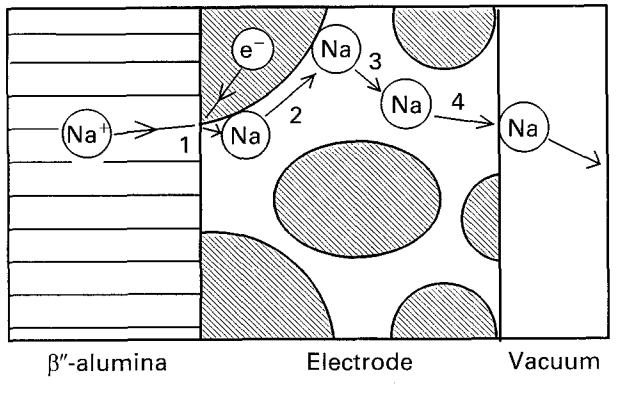

Fig. 12. Schematic representation of the electrode reaction.

1. Charge transfer at the triple-phase boundary.
2. Surface diffusion of sodium on the electrode.
3. Desorption of sodium from the electrode surface.
4. Vapour phase diffusion in the pores of the electrode.

It has been reported that mass transfer process is important in some electrodes [12]. In the present work, it is also recognized that both kinetic and mass transport processes are important from the impedance plots as shown in Fig. 10. In the low current density region under high vacuum level, however, charge transfer process may be rate-determining, since (a) the relation between current density and cathodic overvoltage was linear (Figs 6 and 8), (b) three TiC electrodes (TiC–1, 2 and 3) with different structure gave the very close activation energy for the exchange current density (Fig. 7), and (c) the same situation as (b) was observed on two molybdenum electrodes prepared by markedly different method (Fig. 7). On the other hand, the facts that (d) current density-cathodic overvoltage relation deviates from the Tafel relation at high current density (Fig. 9), (e) a second arc appears in complex impedance plot at high current density (Fig. 10), and (f) power density decreases at low vacuum levels suggests strongly that mass transport through the electrode may be rate-determining step in high current density region or under low vacuum level.

4. Conclusions

Ceramic electrode for AMTEC can be prepared by a screen printing method from ceramic powder. TiN and TiC can be used for AMTEC electrodes instead of molybdenum.

Acknowledgement

This work was supported by a grant-in-aid for Scientific Research on Priority Areas of the Ministry of Education, Science and Culture in Japan. The authors wish to thank Japan New Metals Co., Ltd for kindly supplying the TiC/TiN sample. The complex impedance analysis was made using a frequency response analyser at the Center of Advanced Instrumental Analysis, Kyushu University.

References

[1] T. Cole, *Science* **221** (1983) 915–920.
[2] J. V. Lasecki, R. F. Novack, J. R. McBride, J. T. Brockway and T. K. Hunt, *22nd Intersociety Energy Conversion* Engineering Conference **III** (1987) 1408.
[3] C. P. Bankston, T. Cole, R. Jones and R. Ewell, *J. Energy* **7** (1983) 442–448.
[4] C. P. Bankston, R. M. Williams, B. Jeffries-Nakamura and T. Cole, *22nd Intersociety Energy Conversion Engineering Conference* **III** (1987) 1423.
[5] T. Masuda, A. Negishi and K. Tanaka, *Denki Kagaku* **55** (1983) 197–199.
[6] R. M. Williams, G. Nagasugramanian, S. K. Khanna, C. P. Bankston, A. P. Thakoor and T. Cole, *J. Electrochem. Soc.* **133** (1986) 1587–1595.
[7] O. Asakami, K. Tsuchida, T. Togawa and A. Kato, *J. Mater. Sci. Lett.* **8** (1989) 1141–1143.
[8] O. Asakami, K. Shibata, T. Hashimoto, H. Nakata, K. Tsuchida and A. Kato, *26th Intersociety Energy Conversion Engineering Conference* V (1991) 469–474.
[9] K. Shibata, K. Tsuchida and A. Kato, *J. Less-Common Metals* **157** (1990) L5.
[10] M. L. Underwood, R. M. Williams, B. Jeffries-Nakamura, M. A. Ryan and D. O'Connor, *Proc. Electrochem. Soc.* **91–6** (1991), 88–102.
[11] M. L. Underwood, R. M. Williams, B. Jeffries-Nakamura, C. P. Bankston and T. Cole, *23rd Intersociety Energy Conversion Engineering Conference* I (1988) 227–233.
[12] R. M. Williams, B. Jeffries-Nakamura, M. A. Ryan, M. L. Underwood, D. O'Connor, and S. Kikkert, *27th Intersociety Energy Conversion Engineering Conference* **III** (1992) 19–24.